Continuous 2D X-ray Digital Image Correlation to Resolve Dynamic Deformation and Strain Fields of Internal Planes

Stéphane Magnan[1]*, Tong Xu[2], Oren E. Petel[1]

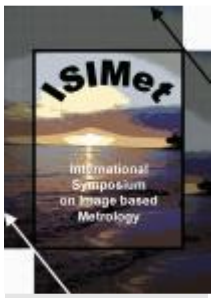

ISIMet 2

International Symposium on Image based Metrology

Hawaii, Maui

December 16-21 2017

Abstract

The study of displacement and strain fields is critical to the proper characterization of a material's mechanical properties. Digital Image Correlation (DIC) is a widely used technique for quantifying surface deformations in a variety of mechanical applications. Although it is most common to apply white paint then black speckles on a specimen surface then imaging and applying DIC, this method has been expanded to include the study of optically inaccessible internal planes using X-ray imaging. Contrast is generally created by embedding speckles of a different material such as lead shavings or tungsten beads in the primary matrix. Although this method allows for visualization of displacements using X-ray DIC, embedding incompatible speckles in the bulk material influences the overall behavior and mechanical response. This effect is especially noticeable in dynamic applications where density coupling is critical to uniform internal accelerations and where interface debonding can occur. Therefore, it is preferable to define speckle attenuation and thickness such that minimum contrast requirements are met. Under this condition, the effect of speckles on bulk material properties is minimized. In this work, speckles were designed using the same base material as the primary matrix, with controlled doping to locally increase the density. Finally, a method of sizing speckles and determining doping quantity required for a minimum contrast to noise ratio is presented. This method allows for the embedding of speckles that will minimally affect the primary material's mechanical properties in quasi-static and dynamic loading conditions while maintaining sufficient visibility.

Keywords

X-ray — Digital Image Correlation (DIC) — Internal Planes

[1]*Department of Mechanical and Aerospace Engineering, Carleton University, Ottawa, Canada*

[2]*Department of Physics, Carleton University, Ottawa, Canada*

*__Corresponding author__: stephane.magnan@carleton.ca

INTRODUCTION

Digital Image Correlation (DIC) has been widely implemented to characterize external surface displacement and strain fields in a wide variety of applications ranging from quasi-static to ballistic velocity dynamic loads [1,2]. For these measurements, correlation is performed between multiple consecutive images captured by one camera for 2D measurements or stereo-cameras to additionally quantify out of plane movement [3]. Features such as painted speckles, must generally be added to the surface to facilitate correlation [3,4]. However, surface etching or natural surface defects can provide adequate contrast for tracking in certain applications [3,5].

Although DIC has been extensively used for surface measurements, it can also be used to analyze images of optically inaccessible internal planes [1,6]. The fundamental approach to DIC, including speckle size and distribution, and subset specifications depend on the images and not the image acquisition technique. Therefore, alternative imaging approaches, such as ultrasound and X-ray may be used to image optically inaccessible planes.

For DIC, speckles are often painted black dots on a white surface to maximize contrast in the images. Imaging internal planes using X-ray, requires an alternate approach to create contrast. The intensity of X-ray waves incident on the sensor must vary to create contrast. In typical applications, the X-ray source emits relatively uniform beams, therefore X-ray attenuation must vary within the material to view internal structures, where X-ray attenuation depends on the probability of atomic interactions [3]. Therefore, the attenuation is a function of material density, atomic composition, and depth of penetration [3]. For this reason, X-ray DIC applications typically track different materials within the original medium. This can include contrast between the bulk material and air, such as cracks, voids, or air pockets in metal foams [5,8,9]. Alternatively, contrast may be created by embedding speckles within the primary specimen [1,6,10].

For natural contrast analyses, such as crack growth or void collapse, no artificial markers are needed, therefore the actual physical process is captured. In other cases, artificial contrast markers are required. Several combinations have been used in prior work, including lead fillings in polyester [1], borosilicate glass beads in polymethyl methacrylate [5], or tungsten beads in aluminum [10], among others. When contrast is produced by embedded the contrast agent material into the primary specimen, an additional challenge not present in standard optical DIC of painted speckles arises. The images captured may not represent the natural material response, since the additional speckles may inadvertently influence material properties [7]. As a result, care must be taken to select contrast agents that provide sufficient contrast, while minimally altering the bulk material response.

Proper design of contrast speckles requires that the

following two criteria be satisfied. First, the speckles must be visible.[7] To achieve proper visibility, the speckles must be larger than the minimum spatial resolution of the imaging system (i.e., span at least one pixel) and provide sufficient contrast (i.e., attenuation difference) from the bulk material.

The second requirement is that speckles should not move relative to the bulk material. This condition implies that speckles used for DIC tracking actually reflect the displacement of the material within the imaging plane. A result of this latter condition, when morphology-dependent tracking algorithms are used, is that the speckle shape must remain relatively unchanged for proper correlation [7]. Additionally, if the tracking is dependent on morphology, the shape changes must also be distinguishable in the imaging system [7]. Due to these requirements, the embedded speckles are often made of a material harder than the original.

Complications arise due to the fact that speckle materials will inherently change its properties and behaviour. Therefore, it is essential that speckles be designed to minimize their effects on material behaviour. This is particularly important due to the tendency in the literature to select spherical contrast materials that are harder than the bulk medium, which may reinforce the bulk material [7].

The coupling between contrast speckles and the bulk material become even more important under dynamic loading conditions. In particular, density-dominated dynamic coupling (i.e., relative internal acceleration) and interface debonding must be considered. Either of these scenarios violate the second condition, as the movement of speckles must accurately reflect the actual specimen displacement.

In the present study, a method proposed for adding high-contrast minimally obstructive speckles into a bulk elastomeric specimen is described. The specimen is deformed and time-resolved images are taken of the specimen. The displacement and strain profile of the deformed specimen is shown and discussed in reference to an optimization scheme for the contrast agents in this experimental system.

1. METHODS

The experimental procedure is described in two parts: the specimen creation and image acquisition. The elastomer specimen was created with embedded contrast-generating speckles for X-ray imaging. In order to maintain dynamic compatibility, the speckles were primarily composed of the same elastomer as the bulk specimen. However, a dopant was added to the speckles to increase their density to produce X-ray contrast. Images were simultaneously acquired using both radiographic and optical methods and subsequently analyzed using DIC software.

1.1 Specimen Preparation

The primary objective for specimen design was to embed contrast speckles in an internal plane while minimally affecting material properties. Speckles were created by doping Sylgard 184 with 39% weight barium sulfate ($BaSO_4$). The doped mixture was fully cured as an approximately 1 mm thick sheet. This sheet was subsequently cut into irregular shapes 2-3 mm across to form the speckles and set aside to be embedded in the specimen at a later time.

The specimen, formed of pure Sylgard 184, was poured into a 50x300 mm open mould with a cylindrical core to form a central 17 mm diameter hole. A first 3 mm thick layer was poured into the mould and allowed to partially cure. The previously produced doped speckles were then randomly placed but evenly distributed and pressed into the partially cured Sylgard to ensure bonding. Finally, a second 3 mm thick layer was poured to encase the speckles in an internal plane and left to cure.

Sylgard 184 is a colorless transparent material, however the addition of $BaSO_4$ changes the optical properties to light brown and opaque. The natural transparency allows for, tracking of the internal speckles using optical imaging. This allows for a direct optical versus radiographic validation comparison. Although optical imaging may be used in this analysis, there are other applications of embedding particles in opaque media or internal structures where X-ray DIC would be required. The full specimen including doped speckles is shown in Figure 1.

Figure 1. Image of specimen showing optical characteristic variations of speckles and matrix

1.2 Image Acquisition

The specimen was loaded into a tensile displacement apparatus and deformed cyclically at a maximum strain rate of 0.075 s^{-1}. Images were simultaneously captured using X-ray and optical methods.

The radiographic imaging set-up consisted of a 150 kV rotating anode X-ray generator, and a flat panel detector (XRD 0840 AN13). The X-ray imaging rate was 15 fps, with a 66 ms integration and capture time. A schematic of our experimental set-up is shown in Figure 2.

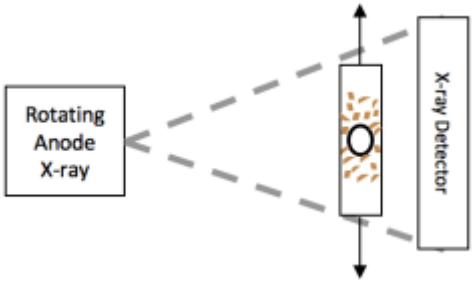

Figure 2. Experimental set-up of X-ray imaging.

The experiment consisted of a validation of the X-ray contrast speckle technique using optical and radiographic imaging. For this experiment, a continuous optical video was

recorded simultaneously to the x-ray imaging. The optical videos were analyzed simultaneously and compared. Due to differences in framing rates, analyzing select frames allowed for a relative displacement analysis between the two imaging processes using DIC. The comparison is not perfect given that the optical recoding was taken at 30 frames/s and the radiographic images were captured at 15 frames/s. Therefore, every second optical frame was analyzed to compensate for the difference in frame rates. The X-ray detector is an integral detector with shutter speeds similar to frame rate. Therefore, corrections in frame rate do not account for differences in shutter speeds between methods.

2. RESULTS AND DISCUSSION

The method described in Section 1 was implemented to capture simultaneous optical and radiographic images. Using the Ncorr DIC software [8], the two methods were compared as a means of validation. The discussion will also include a method of approximating required speckle characteristics to meet contrast requirements thus minimally affecting bulk material properties.

2.1 Photography/Radiography Comparison

The analysis consisted of using Ncorr open-source DIC software to compare images simultaneously captured using optical and X-ray imaging. The images, with system specific resolution, were compared using equivalent DIC parameters (i.e., subset size compared to image pixels). Figure 3 illustrates the axial and lateral displacement fields for both methods.

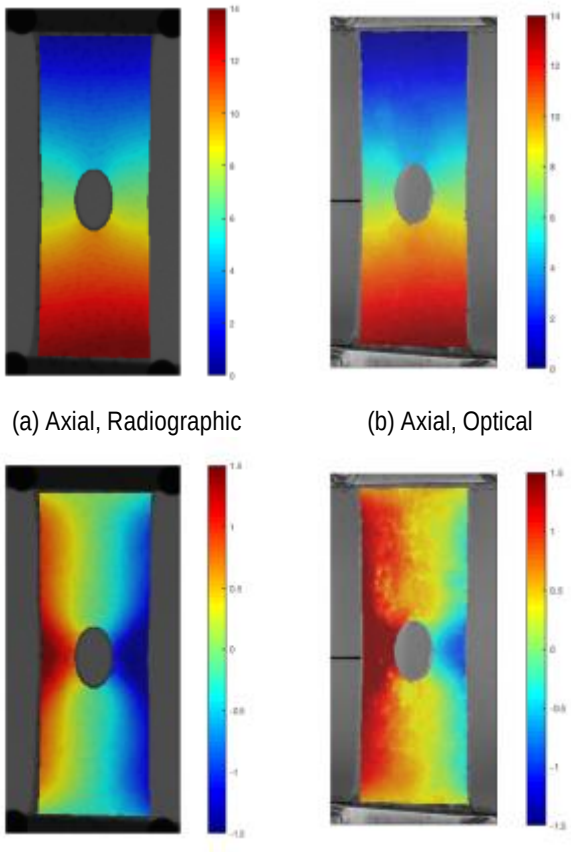

(a) Axial, Radiographic (b) Axial, Optical

(c) Lateral, Radiographic (d) Lateral, Optical

Figure 3. Lateral and transvers displacement fields for radiographic and optical tests

As seen in Figure 3, the axial displacement plots (a-b) are quite similar, with only slight variations. The magnitudes of displacement appear to be identical with the same behaviour around the stress concentrator. The only notable difference is the presence of some noise in the optical image above and below the through-hole compared to a very smooth displacement field in the X-ray image. The most likely cause for this is simply a far from ideal optical DIC surface. Typically, a non-reflective white base with black speckles would be used. Here it is a reflective surface with possible distortion before and after light reaches the internal speckles used for optical and radiographic DIC. The lateral displacement varied more noticeably between the two image types (c-d). Although the same tendencies are visible, there is a translation of the displacement field from symmetric in the X-ray image to asymmetric in the optical image. Capturing X-ray and optical images simultaneously meant not having identical fields of view for both sensors. Therefore, one possible explanation for the lateral displacement shift is improper alignment between the camera and specimen, giving illusion of slightly different displacements due to uneven magnification. There is also an increase in noise visible in the optical images, most likely due to ambient light reflecting unevenly off the specimen surface. Building on this idea, the edges of the specimen adhered to the mould during curing, resulting in non-planar surfaces which could unevenly reflect light. Further, out of plane motion captured in the optical imaging method and the uneven surface could be creating noise, but these artefacts would not occur in the X-ray images of the internal plane. The nature of the sensor used and lack of noise could explain why the radiographic images are smoother. Despite the differences, the overall trends are in agreement for either method. Using these displacement fields, the strain plots were then determined and are shown in Figure 4.

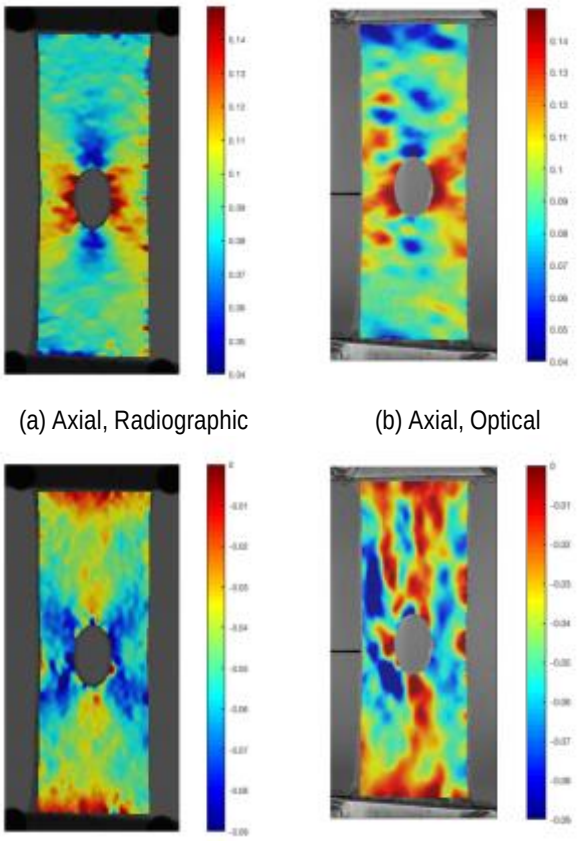

(a) Axial, Radiographic (b) Axial, Optical

(c) Lateral, Radiographic (d) Lateral, Optical

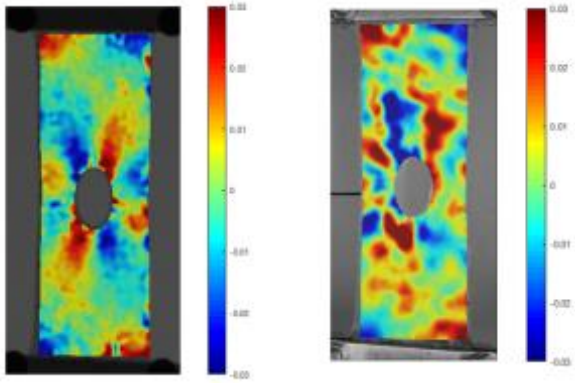

(e) Shear, Radiographic (f) Shear, Optical

Figure 4. Lateral, transverse and shear strain fields for radiographic and optical tests

The strain plots vary more significantly between the imaging methods than the displacement fields. There are notable differences in noise levels between the methods. Strain corresponds to the differentiation of displacements. Differentiation methods are inherently very sensitive to noise. Therefore, as the radiographic displacement fields were smoother, their corresponding strain fields were also less noisy than the optical results (Figure 4).

The trends in both the axial and lateral strains are quite comparable across imaging methods. For example, the distinct '*x*' distribution around the stress concentrator is apparent in Figure 4a-4d. Similarly, the regions directly above and below the hole contrast with the '*x*' in both cases. These results are sufficiently similar when taking into account the effects of noise in the original optical images. Although the optical shear strain (e) does not appear to match the radiographic image (f) at first glance, a closer examination shows that the distinct asymmetric '*x*' is present here as well, with positive and negative shear strains and their maxima occurring in comparable regions.

There are noticeable differences in quality of the DIC fields implemented on these radiographic and optical images. Overall, the trends proved to be comparable for the coupled photographic and radiographic DIC analyses. This is taken as a constructive step towards future implementation of this technique, moving to simultaneous bimodal imaging of uncoupled internal and external planes, with future consideration for improving the optical DIC surface for better correlation.

2.2 Speckle Size Optimization

Artificial speckles should be optimized prior to being embedded in the specimen in order to provide minimum sufficient contrast and minimizing their effect on material properties. This is achieved by tuning dopant concentration and speckle thickness required for a desired signal to noise ratio (SNR). This concept is represented graphically using a descriptive diagram (Figure 5) to determine minimum speckle characteristics to generate the necessary SNR.

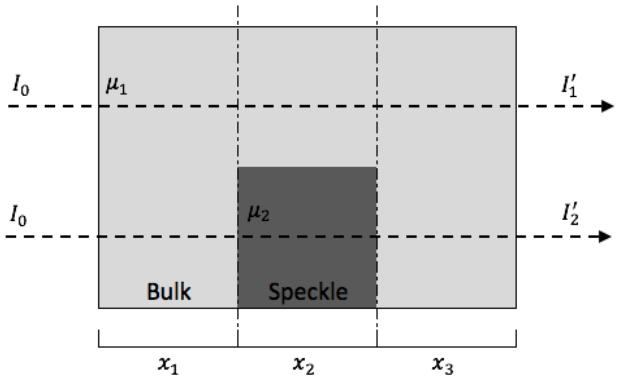

Figure 5. Diagram of X-ray attenuation through the bulk medium in regions with and without speckles. μ_1 and μ_2 are the x-ray attenuation coefficients of the bulk material and speckle respectively.

The 2D illustration in Figure 5 represents two identical incident beams passing through a uniform cross-section and a cross-section containing a contrasting speckle. To properly track and identify the speckles after the image acquisition phase, they must be sufficiently visible. In this analysis, sufficiently visible will be defined as having a contrast to noise ratio above a certain threshold, defined as SNR_{min}. This criterion combined with an analysis of the above diagram will provide the basis for the proposed method. The tunable parameters are the speckle thickness and dopant concentration. The signal to noise ratio is defined as follows:

$$SNR = \Delta I/\sigma \tag{2}$$

where ΔI is the contrast between the speckled and non-speckled trajectories and σ is the signal noise. In the current context, considering the threshold required for proper speckle tracking, equation (2) becomes

$$\frac{I_1'\text{-}I_2'}{\sigma(I_1')} \geq SNR_{min} \tag{3}$$

where I_1' and I_2' are the spectral intensities of the beams transmitted through the bulk material without and with the speckle, respectively, as shown in Figure 5. The noise associated with the beam passing through the bulk material is $\sigma(I_1')$.

For X-ray detector systems that include a scintillator, the measured intensity actually corresponds to spectral energy incident on the sensor. Therefore, the intensity is dependent on the total energy fluence, defined as the sum of products between the energy specific photon fluence, $\phi(E_i)$, and the associated energy, E_i.

$$I = \sum_i \phi(E_i)E_i \tag{4}$$

Using equation (4), equation (3) is further expanded to

$$\frac{\sum_i \phi_1(E_i)E_i - \sum_i \phi_2(E_i)E_i}{\sigma(I_1^{'})} \geq SNR_{min}, \quad (5)$$

where the photon fluence at energy E_i along path *k* in Figure 5 is $\phi_k(E_i)$. The transmitted photon fluence is dependent on beam filtration caused by X-ray attenuation through *j* materials of thickness *x* via the following relation.

$$\phi(E_i) = \phi_0(E_i) \prod_j \exp\left(-\mu_j(E_i)x_j\right) \quad (6)$$

Therefore, if filters and other sources of X-ray attenuation are ignored, and only the mediums shown in Figure 5 are considered, the relationship between the transmitted and incident photon fluence, $\phi_0(E_i)$, along either path becomes:

$$\sum_i \phi_1(E_i) = \sum_i \phi_0(E_i) \exp\left(-\mu_1(E_i)(x_1 + x_2 + x_3)\right), \quad (7)$$

and

$$\sum_i \phi_2(E_i) = \sum_i \phi_0(E_i) \exp\left(-\mu_1(E_i)(x_1 + x_3) - \mu_2(E_i)(x_2)\right). \quad (8)$$

The incident photon fluence is determined by scaling the raw spectral power by the air kerma to account for exposure time, current, frame rate, and other set-up specific parameters. The photon fluence $\phi(E_i)$ follows a Poisson distribution, where the variance of energy fluence can be written as:

$$\sigma^2 = \sum_i \phi(E_i)\, E_i^2 \quad (9)$$

Finally, combining equations (3), (7), (8), and (9), and redefining lengths $x_1 + x_2 + x_3 = x_{bulk}$ and $x_2 = x_{spec}$, results in the following expression:

$$\frac{\left(\begin{matrix}\sum_i \phi_0(E_i) \exp\left(-\mu_1(E_i)(x_1+x_2+x_3)\right)E_i - \\ \sum_i \phi_0(E_i) \exp\left(-\mu_1(E_i)(x_1+x_3) - \mu_2(E_i)(x_2)\right)E_i\end{matrix}\right)}{\sqrt{\sum_i \phi_0(E_i) \exp\left(-\mu_1(E_i)(x_1+x_2+x_3)\right)E_i^2}} \geq SNR_{min} \quad (10)$$

Therefore, the optimized the speckle characteristics for an arbitrary specimen at a threshold SNR level, are given by equation (10).

Next, it is assumed that the speckles are being embedded into a specimen of known properties (i.e., material and dimensions). Therefore, both x_{bulk} and $\mu_1(E_i)$ are constants. This leaves two unknown variables describing the speckles, $\mu_2(E_i)$ and x_{spec}, that will be used to tune the speckle characteristics. In our application, where the speckles are primarily composed of the same material as the bulk specimen with the controlled addition of a dopant, we are able to control speckle attenuation, $\mu_2(E_i)$, approximating its value using the XCOM Photon Cross Sections Database [3]. The presence of a second unknown, x_{spec}, indicates that there are an infinite number of solutions to this equation, however it is possible to further constrain this value. At all times, we know that $x_{spec} \leq x_{bulk}$, but in the case of a thick specimen, thin speckles would still be preferred because we are imaging a single plane. If the speckles were too thick, alignment and non-uniform strain fields throughout the specimen could affect the quality of DIC measurements. Further studies into the optimization of these two parameters is warranted.

The purpose of this study was to present a method of minimizing the effect of embedded speckles on bulk specimen material properties. Equation (10) provided a lower bound for determining x_{spec} and $\mu_2(E_i)$, this is a trivial minimization problem, where the solution becomes

$$\frac{\left(\begin{matrix}\sum_i \phi_0(E_i) \exp\left(-\mu_1(E_i)(x_{bulk})\right)E_i - \\ \sum_i \phi_0(E_i) \exp\left(-\mu_1(E_i)(x_{bulk}-x_{spec}) - \mu_2(E_i)(x_{spec})\right)E_i\end{matrix}\right)}{\sqrt{\sum_i \phi_0(E_i) \exp\left(-\mu_1(E_i)(x_{bulk})\right)E_i^2}} \geq SNR_{min} \quad (11)$$

Discussion thus far has excluded selection of the minimal signal to noise ratio threshold. This is not an issue encountered in standard optical DIC, as black speckles on white paint are used and speckle size optimization has been well documented. Black paint on a white surface inherently provides the maximum attainable contrast using optical methods, however as discussed in this paper, maximizing contrast with embedded speckles will affect material properties of the bulk specimen, particularly in dynamic applications.

As a result, further analysis regarding determining the proper threshold is required. A preliminary and conservative SNR value of $SNR_{min} = 5$ may be chosen, following the requirement for reliable human vision detectability [9]. Both displacement and strain fields must be considered when determining appropriate the SNR threshold. It should be noted that Equation (10) and (11) are based on an ideal detector assumption. The actual SNR_{min} used may need to be increased to account for the fact that a real X-ray detector will cause some degradation of SNR. An analytical model of the detector system is used to determine its SNR transfer property [14].

The method proposed in this paper and summarized in equation (11) will be used in future designs of speckles to provide sufficient SNR, while minimally affecting bulk material properties. The optimum value is not trivial to determine as the attenuation and speckle thickness present a virtually unconstrained multi-degree-of-freedom problem with infinite possible solutions. The free variables are a strength of this approach, allowing this method to be customizable and adaptable for different applications based on user discretion and are specific to each application. The doping concentration and the thickness of speckles were chosen based on additional criterion such that material properties of the test specimen are only marginally

influenced by the embedded contrast speckles. Therefore, knowledge of the test specimen and its X-ray attenuation response with increasing doping concentration is required. Future work will include a complete study of the minimum signal to noise ratio needed for accurate DIC and the balance between X-ray attenuation differences (i.e., doping concentration), depth of penetration and the effect on material properties.

ACKNOWLEDGMENTS

The authors would like to thank Paul Johns for providing access to the flat panel X-ray detector used in this experiment and Christopher Comtois-Arnaldo for his assistance in specimen preparation. The authors would like to thank the Canadian Institutes of Health Research and the Natural Science and Engineering Research Council of Canada for their financial support of this effort under Grants CPG-151967 and CHRP 508414-17, respectively.

REFERENCES

[1] P. Synnergren, H. T. Goldrein, and W. G. Proud, “Application of digital speckle photography to flash impact experiments,” *Appl. Opt.*, vol. 38, no. 19, pp. 4030–4036, 2000.

[2] T. Goldrein, S. G. Grantham, G. Proud, and J. E. Field, “the Study of Internal Deformation Fields in Granular Materials Using 3D Digital Speckle X-Ray Flash Photography,” vol. 4948, no. Xm, pp. 19–22, 2002.

[3] K. Berger, M.J., Hubbell, J.H., Seltzer, S.M., Chang, J., Coursey, J.S., Sukumar, R., Zucker, D.S., and Olsen, “NIST XCOM: Photon Cross Sections Database (version 1.5). [Online],” 2010. [Online]. Available: https://physics.nist.gov/PhysRefData/Xcom/Text/version.shtml. [Accessed: 13-Jul-2017].

[4] L. Lu *et al.*, “Note: Dynamic strain field mapping with synchrotron X-ray digital image correlation,” *Cit. Rev. Sci. Instruments*, vol. 85, no. 76101, 2014.

[5] Y. Hangai *et al.*, “Nondestructive observation of pore structure deformation behavior of functionally graded aluminum foam by X-ray computed tomography,” *Mater. Sci. Eng. A*, vol. 556, pp. 678–684, 2012.

[6] S. C. Wu and Z. Song, “Recent progress on failure mechanism of structural materials via synchrotron radiation X-ray microtomography,” *Front. Mech. Eng. China*, no. December, 2016.

[7] K. Haldrup, S. F. Nielsen, and J. A. Wert, “A General Methodology for Full-Field Plastic Strain Measurements Using X-ray Absorption Tomography and Internal Markers,” *Exp. Mech.*, vol. 48, pp. 199–211, 2008.

[8] J. Blaber, B. Adair, and A. Antoniou, “Ncorr: Open-Source 2D Digital Image Correlation Matlab Software,” *Exp. Mech.*, vol. 55, no. 6, pp. 1105–1122, Jul. 2015.

[9] A. Rose, “The Visual Process,” in *Vision*, Boston, MA: Springer US, 1973, pp. 1–27.